Supporting Information for "Oceanic stochastic parametrizations in a seasonal forecast system"

Introduction

Here we include diagnostics for sea surface temperature (SST) and sea surface salinity (SSS) for the three stochastic schemes: the stochastic equation of state (SES), the stochastic surface flux (SSF) and the Stochastically Perturbed Parameterization Tendency (SPPT). Additionally, we illustrate the impact of reducing the timescale for the generation of the random numbers on the upper ocean heat content for (SPPT). We also briefly discuss two initial implementations of a stochastic Gent McWilliams scheme.

As mentioned in the paper, the criteria for which information is distinguished from noise is given by

$$m > \frac{2\sigma}{\sqrt{n}}, \tag{1}$$

where m is the ensemble mean difference between a stochastically perturbed and a control integration, σ is the ensemble standard deviation of the difference and $n = 10$ is the number of independent samples, assuming that the model state is independent from one year to the next.

Corresponding author: L. Zanna, Atmospheric, Oceanic and Planetary Physics, Department of Physics, University of Oxford, Oxford, OX1 3PU, UK. (laure.zanna@physics.ox.ac.uk)

Stochastic Schemes Diagnostics: Global maps of the bias in SST and SSS (Figures 1a and 2a, respectively) of the control integration with respect to reanalysis are broadly consistent with the bias in upper ocean heat content (Fig. 1a in the manuscript). The impact of the SSF and SES on the SST and SSS biases is weak and patchy (panels b and c of Figs 1 and 2). The largest impact of SPPT on SST and SSS biases (panel d of Figs 1 and 2) is found in parts of the Southern Ocean, parts of the Tropics and in the vicinity of western boundary currents and their extension, in agreement with the results obtained for upper ocean heat content. The impact of the SPPT scheme on the bias in SSS is also evident at high latitudes but the presence of sea-ice is likely to play a role in this change. Random numbers were applied over a $30^o \times 30^o$ latitude longitude grid which accounts for the grid-like pattern in some of the plots.

Global maps of SST and SSS variance are shown in panel a of Figs. 3 and 4. Again the impact of SSF and SES schemes on the ensemble variance of SST and SSS (panels b and c in Figs. 3 and 4) is negligible. The impact of the SPPT scheme on the ensemble spread of SST and SSS is noticeable in the regions of the Gulf Stream and Kuroshio and parts of the Southern Ocean. The SPPT scheme appears to also largely affect the SSS in the Tropics.

Figure 5 shows the area-averaged temporal evolution of the bias for the different simulations. The SST bias in the Southern Ocean (panel c) remains unchanged when the different stochastic schemes are applied to the model. The SPPT scheme slightly increases the SST bias in the North Atlantic subpolar and subtropical regions (panels a and b) while the SES scheme leads to a small reduction in the SST bias in both regions, however the large spread in the ensemble mean for each of the 10 years translates in low confidence.

The SPPT scheme significantly increases the SST ensemble spread (Fig. 6a) in the North Atlantic and the SSS ensemble spread in the Southern Ocean (Fig 7a). The impact of SES and SSF on the ensemble spread is small (panels b and c in Figs. 6 and 7). Despite the increase in ensemble spread due to SPPT, the forecast mean square error is not significantly reduced, except perhaps around day 20 for the North Atlantic subpolar SST and the Southern Ocean SSS (Figs. 6d and 7d).

Maps of correlation scores between ensemble mean and observed SST for the control and SPPT experiments are shown in Fig. 8. The correlation is computed at each grid point over 10 years only, therefore resulting in large uncertainties. The maps show the familiar pattern of high skill in the tropics, in particular the tropical Eastern Pacific, and reduced skill in mid-latitudes. In agreement with our other findings, we cannot detect any significant differences in skill with the SPPT scheme given the large sampling uncertainty and the overall small impact found.

Impact of the random number timescale: Figure 10 shows the ensemble spread and forecast mean square error due to SPPT, when the random numbers are selected every day rather than every 30 days, for the upper ocean heat content in the 3 regions defined in the text. It appears that the shorter decorrelation timescale leads to broadly consistent results compared to those described in Fig.3 of the paper however with a reduced amplitude.

Stochastic Gent-McWilliams Schemes: In addition to SPPT, SSF, SES, a stochastic GM scheme was implemented. The stochastic GM scheme is defined by perturbations to the GM non-divergent eddy velocity components u_{GM}, v_{GM} and w_{GM}, which are multiplied by $(1 + r)$ as in Section 2.3 and used in the tracer equations for temperature (Eq. 3) and salinity. The same random numbers were applied equally to each of the 42 ocean model

levels. In a first implementation, the spatial field of random numbers was applied equally to u_{GM}, v_{GM} and w_{GM}. The random numbers were drawn from a uniform distribution between ± 0.05 at 1 day intervals or ± 0.025 at 30 day intervals. In a second implementation, each component of $\mathbf{U}_{\mathrm{GM}}$ received a different random number r_X, $X \in \{u_{\mathrm{GM}}, v_{\mathrm{GM}}, w_{\mathrm{GM}}\}$. The first implementation, which perturbs the entire velocity vector U_{GM} with a random number, leads to a violation of the non-divergence property of $\mathbf{U}_{\mathrm{GM}}$ along the boundaries of the $30^{\mathrm{o}} \times 30^{\mathrm{o}}$ degree grid boxes used for the spatial correlation of the random numbers. This causes unrealistic anomalous upwelling of cold and fresh water, leading to an increase in the bias and ensemble spread along those grid box boundaries. For the second implementation, where all three components of $\mathbf{U}_{\mathrm{GM}}$ are perturbed separately, the non-divergence and adiabatic properties are violated throughout the ocean interior leading to unrealistic upwelling, especially in the Southern Ocean. This triggers further instabilities that spread out into lower and higher latitudes, leading to large biases and forecast errors. In summary, the current stochastic perturbations to the GM scheme are not physically reasonable and need to be adjusted in future experiments.

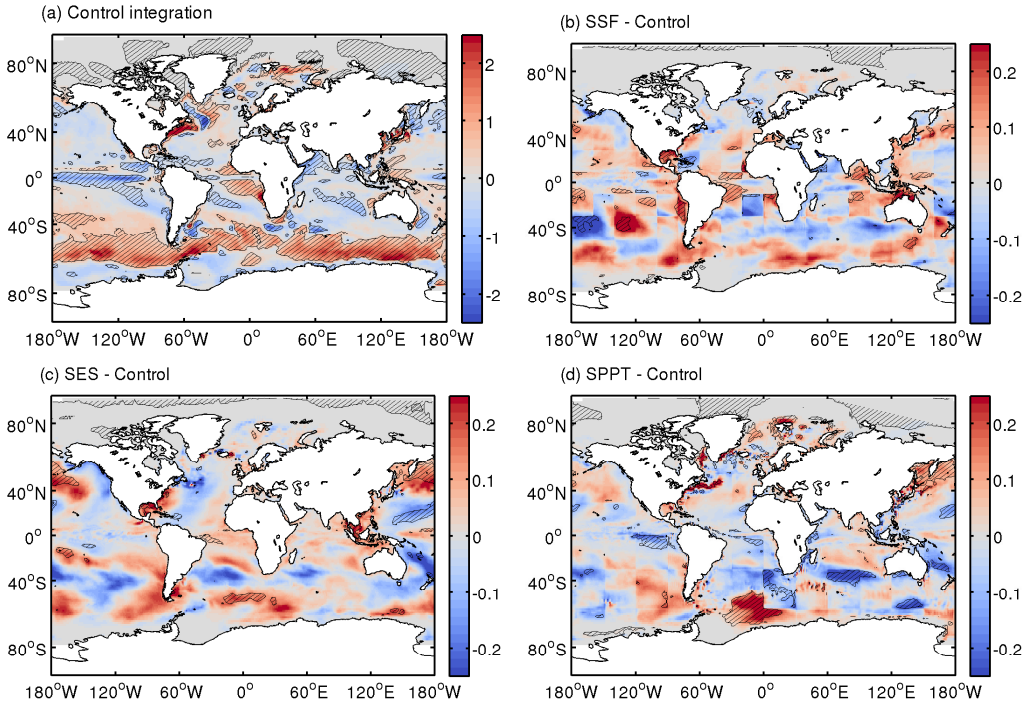

Figure 1. Sea surface temperature (SST) bias (°C) relative to the ECMWF reanalysis, averaged over days 60-90 for the control integration (panel a). Panels b, c, d are the difference in SST bias between integrations using the three stochastic parameterization schemes (SSF, SES and SPPT, respectively) and the control. Hatched areas indicate regions that are distinguishable from zero using equation (1). Note that the control integration plot has a different colour scale.

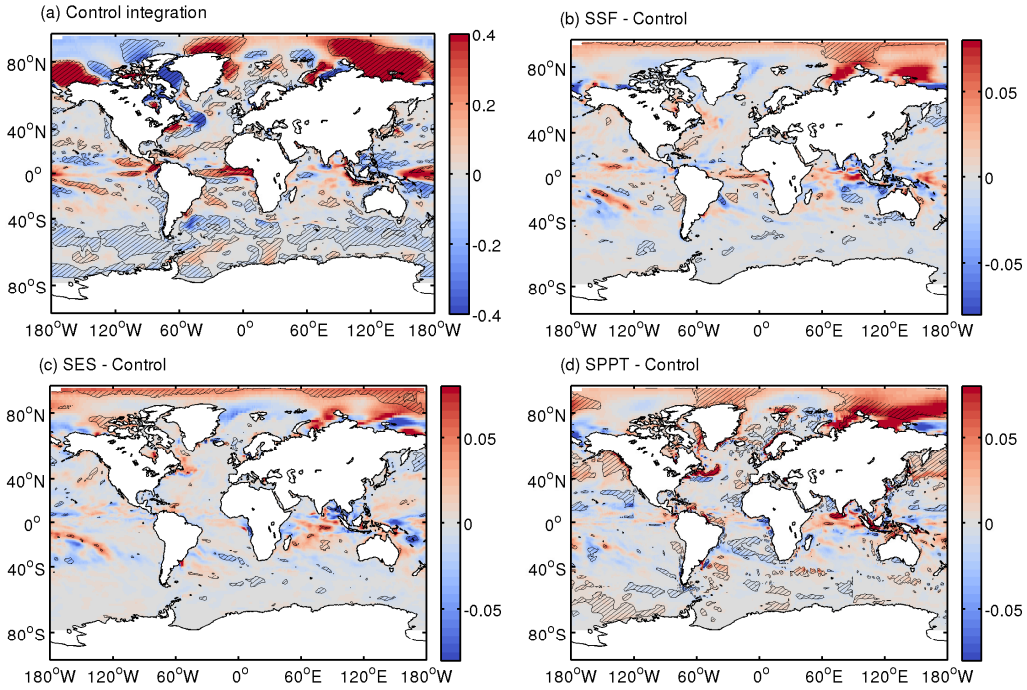

Figure 2. Sea surface salinity (SSS) bias (g kg^{-1}) relative to the ECMWF reanalysis, averaged over days 60-90 for the control integration (panel a). Panels b, c, d are the difference in bias between integrations using the three stochastic parameterization schemes (SSF, SES, SPPT respectively) and the control. Hatched areas indicate regions that are distinguishable from zero using equation (1). Note that the control integration plot has a different colour scale.

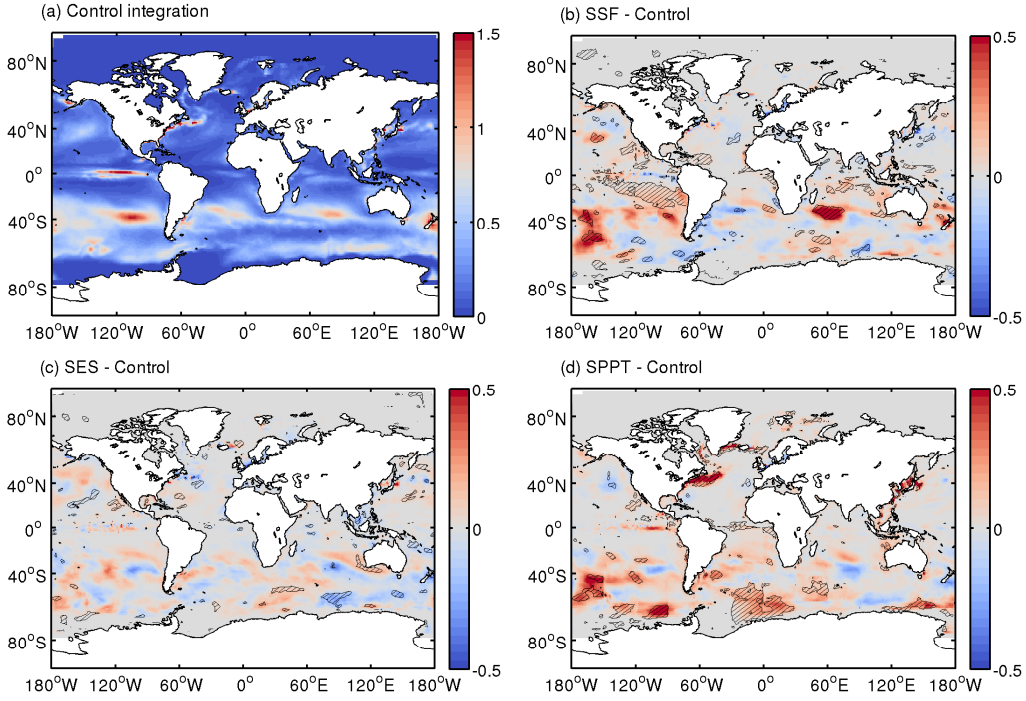

Figure 3. SST ensemble variance (°C) averaged over days 60-90 for the control integration (panel a). Panels b, c, d are the difference in ensemble variance between integrations using the three stochastic parameterization schemes (SSF, SES, SPPT respectively) and the control. Hatched areas indicate regions that are distinguishable from zero using equation (1). Note that the control integration plot has a different colour scale.

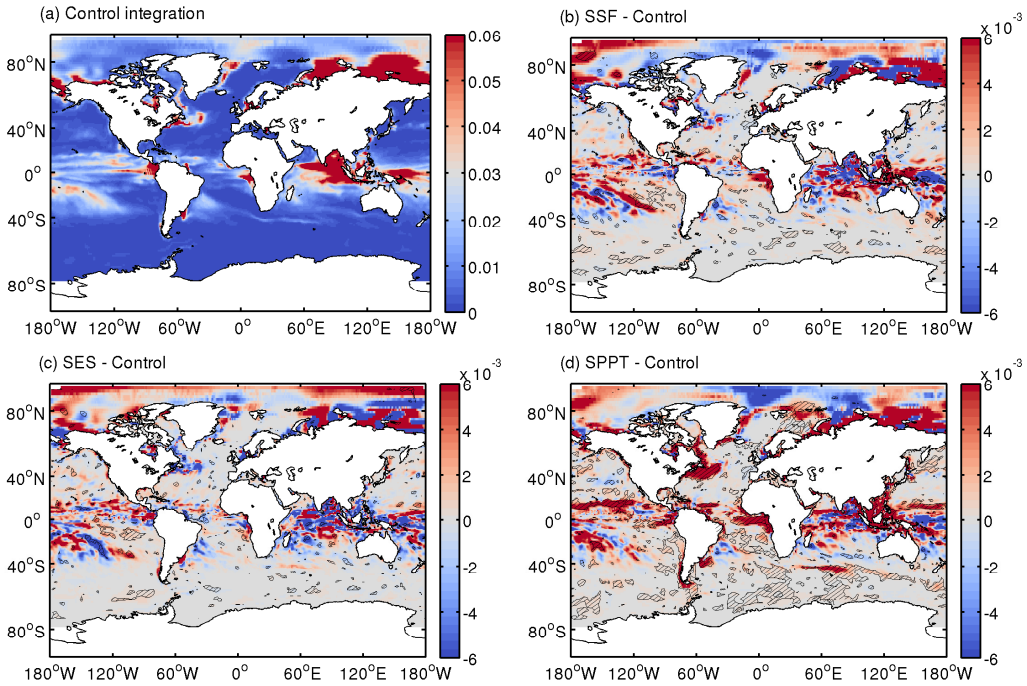

Figure 4. SSS ensemble variance (g^2 kg^{-2}) averaged over days 60-90 for the control integration (panel a). Panels b, c, d are the difference in ensemble variance between integrations using the three stochastic parameterization schemes (SSF, SES, SPPT respectively) and the control. Hatched areas indicate regions that are distinguishable from zero using equation (1). Note that the control integration plot has a different colour scale.

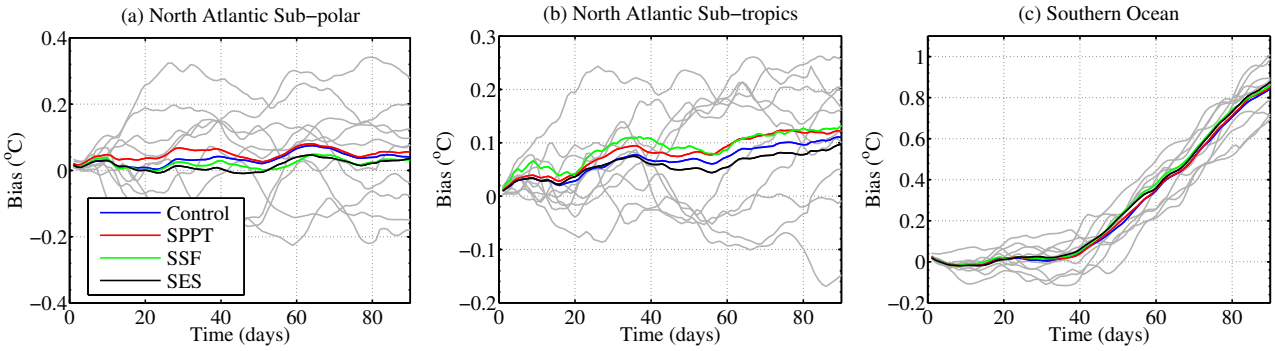

Figure 5. Bias in the SST averaged over three regions (see text for details, equivalent to those in figure 2 in the paper). The coloured lines indicate the ensemble mean bias averaged over all 10 start years for the control integrations (blue), the integrations with SPPT (red), SSF (green) and SES (black). The grey lines represent the ensemble mean bias of the control integration for each of the 10 years. Note the different y axis scales.

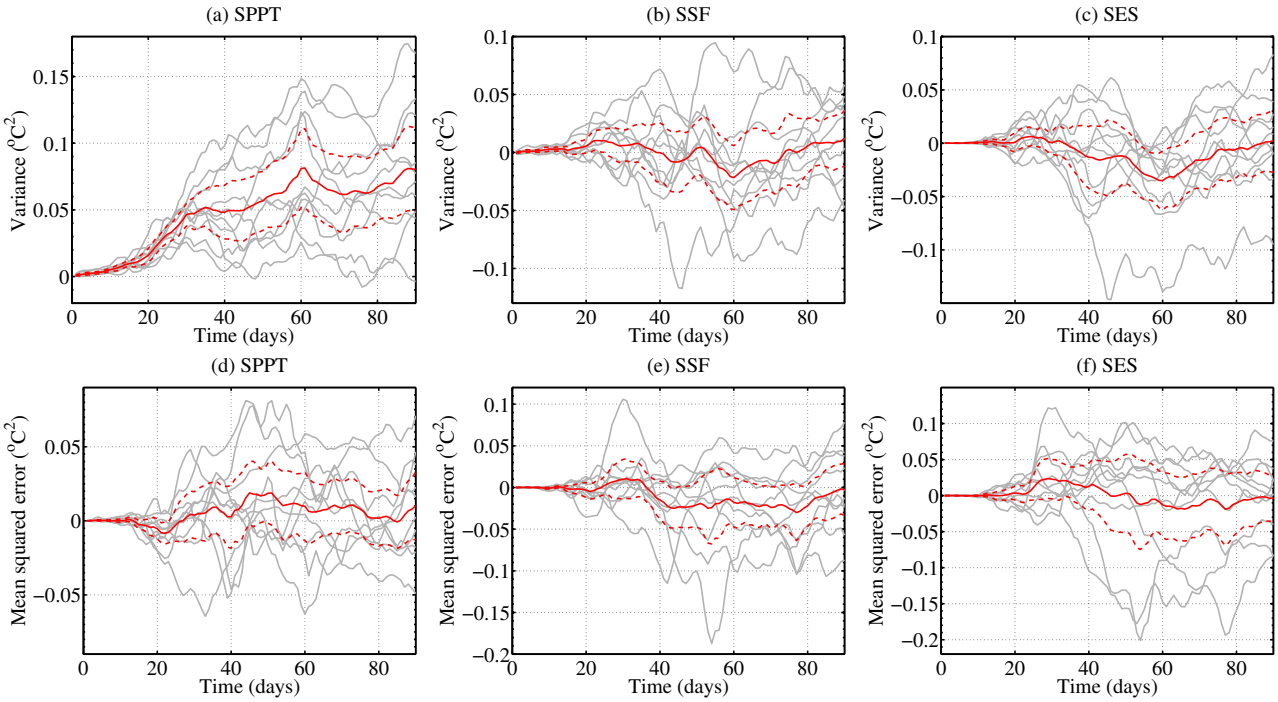

Figure 6. Area averaged changes in the North Atlantic sub-polar SST ensemble spread (top row), and mean squared error (bottom row), with respect to the control integration, due to SPPT (left), SSF (middle) and SES (right). The grey lines indicate the statistics from the ensemble taken over each of the 10 start years. The solid red line indicates the mean over all years and the dashed lines indicate the approximate uncertainty in the mean (the mean plus or minus two standard deviations divided by $\sqrt{10}$).

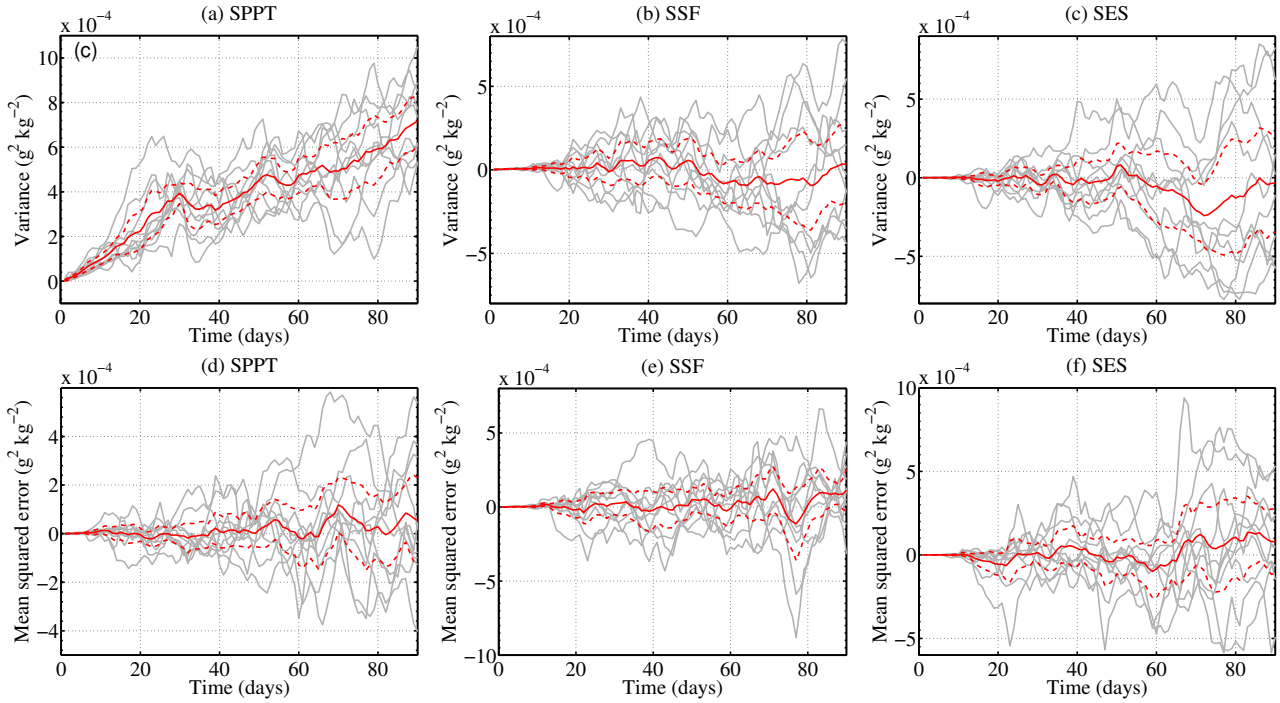

Figure 7. Area averaged changes in the Southern Ocean SSS ensemble spread (top row), and mean squared error (bottom row), with respect to the control integration, due to SPPT (left), SSF (middle) and SES (right). The grey lines indicate the statistics from the ensemble taken over each of the 10 start years. The solid red line indicates the mean over all years and the dashed lines indicate the approximate uncertainty in the mean (the mean plus or minus two standard deviations divided by $\sqrt{10}$).

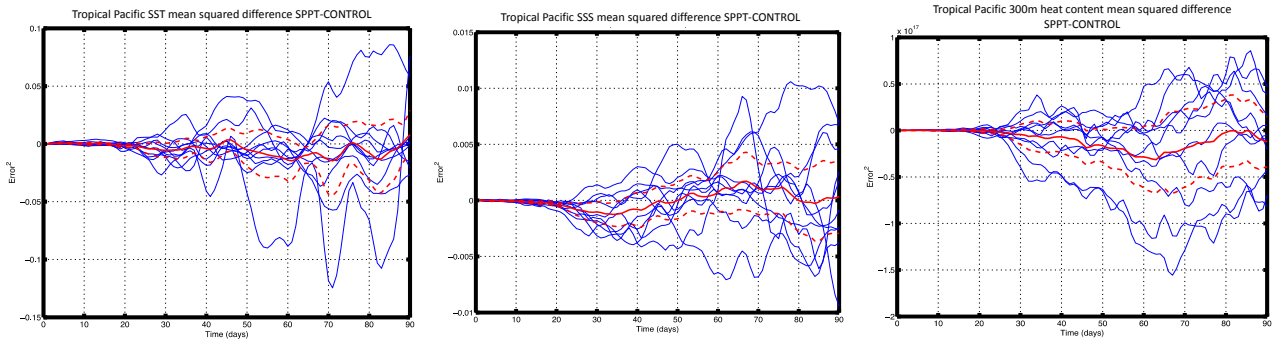

Figure 8. Area averaged changes in the Tropical Pacific (-10N to 10N, 100W to 110E) mean squared error between SPPT and the default integration for SST (left), SSS (middled), 300m upper ocean heat content (right). The blue lines indicate the statistics from the ensemble taken over each of the 10 start years. The solid red line indicates the mean over all years and the dashed lines indicate the approximate uncertainty in the mean (the mean plus or minus two standard deviations divided by $\sqrt{10}$).

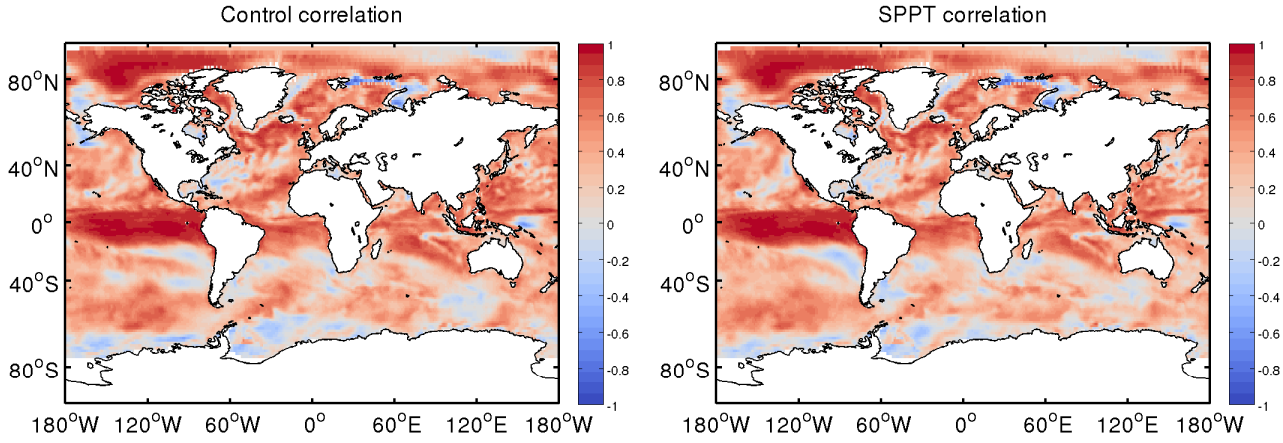

Figure 9. Sea surface temperature 90 day time correlation of the reanalysis with the bias corrected control integration (top left), and SPPT integration (top right).

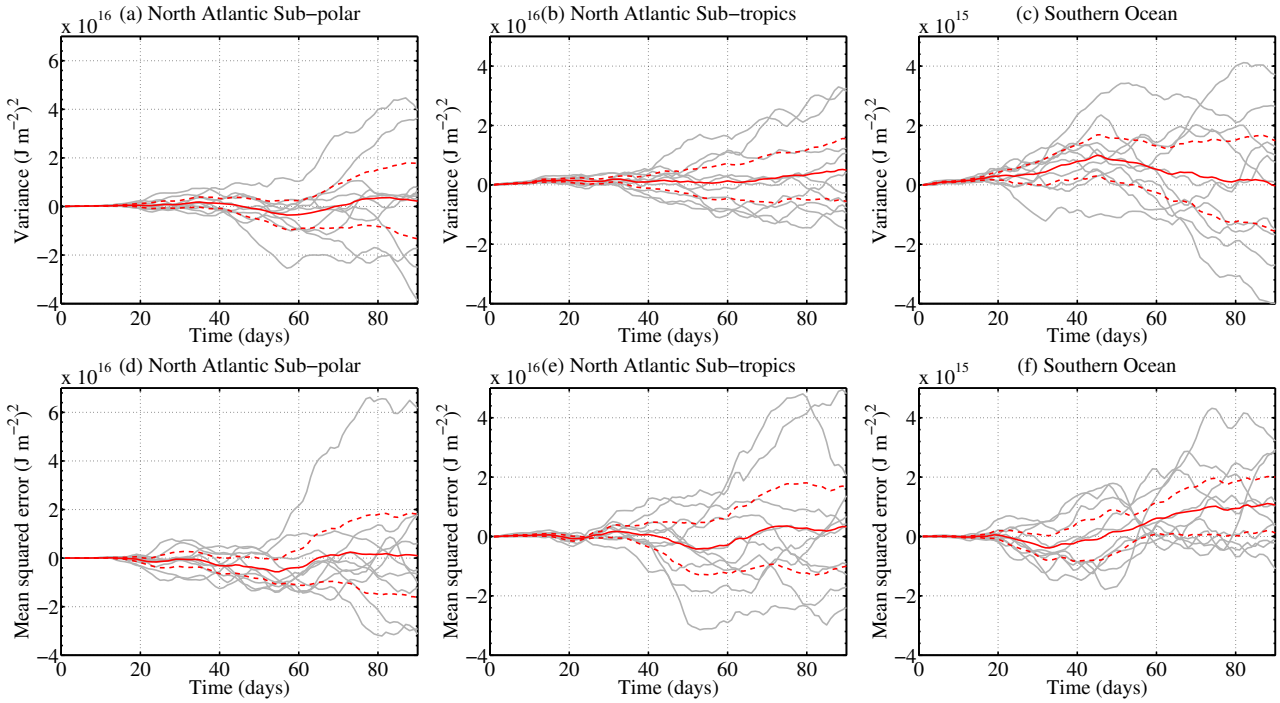

Figure 10. Substituting 1 day between choosing random numbers for the 30 days used in the paper, otherwise equivalent to figure 3 of the paper. Area averaged changes with respect to the control integration, due to SPPT, in the ensemble spread (top row, (a), (b) and (c)), and the mean squared error, (bottom row, (d), (e) and (f)), of the 300m integrated heat content, see text for details. The grey lines indicate the statistics from the ensemble taken over each of the 10 start years. The solid red line indicates the mean over all years and the dashed lines indicate the approximate uncertainty in the mean, (the mean plus or minus two standard deviations divided by $\sqrt{10}$). Note the different y axis scales.